International Forum on Aeroelasticity and Structural Dynamics
IFASD 2024
17-21 June 2024, The Hague, The Netherlands

FLUTTER PREDICTION CORRELATIONS WITH WIND TUNNEL MEASUREMENTS ON A T-TAIL FLUTTER MOCK-UP

Elsa Bréus, Nicolas Forestier, Zdenek Johan and Éric Garrigues

DASSAULT AVIATION
78 quai Marcel Dassault, 92552 Saint-Cloud, France
elsa.breus@dassault-aviation.com

Keywords: flutter, wind tunnel, enhanced DLM, linearized RANS

Abstract: Flutter computations on a T-tail aircraft hold challenges as flutter behavior is significantly driven by specific aerodynamic phenomena. Interactions between tail surfaces have to be computed correctly to predict flutter accurately. Developments were performed at DASSAULT AVIATION to improve in-house solvers for these specific configurations. To validate numerical tools, some reference experimental data are required. To do so, a wind tunnel test mock-up has been designed and manufactured in the frame of CleanSky2 project in cooperation between DASSAULT AVIATION, ONERA and RUAG. This mock-up was tested in 2016 for U-tail configurations [1]. A second wind tunnel test campaign took place in 2022 for T-tail configurations in ONERA S2MA pressurized wind tunnel. Flutter curves have been measured up to the flutter point thanks to an efficient safety system that allowed reaching flutter boundary numerous times without structural damage. The tests, conducted up to Mach 0.925, have shown good repeatability leading to a high confidence in the measurements. Configurations tested consisted in several incidence settings of the horizontal tail plane to cover various lift forces and a dihedral effect. Both effects are of prime importance when computing flutter of a T-tail configuration. These effects therefore call for the need of validation of their numerical predictions. This paper presents correlations between experimental data and numerical computations.

1 INTRODUCTION

In December 2022, a wind tunnel test campaign was performed on a T-tail mock-up in collaboration between DASSAULT AVIATION and ONERA. The tests took place in the ONERA S2MA wind tunnel in Modane. The objective of these tests was to gather a large experimental database of T-tail effects on flutter onset. Indeed computing flutter on T-tail configuration brings new challenges compared to classic cross tail configuration, as it exhibits particular phenomena. With a horizontal tail plane placed on top of the fin, the lever arm with respect to the fin anchoring on the fuselage is increased and all aerodynamic interactions phenomena are of prime importance. Flutter mechanisms are then directly impacted by the horizontal tail plane lift. To compute flutter

precisely both accurate structural and unsteady aerodynamics models are needed. DASSAULT AVIATION reference tools to evaluate unsteady aerodynamics are the well-known Doublet Lattice Method (DLM) and linearized Reynolds-Averaged Navier-Stokes (RANS) methods [2]. Linearized RANS methods have been developed since early 2000's at DASSAULT AVIATION to increase accuracy of flutter prediction when reaching DLM limits (particularly in the transonic domain). DLM is a fast, robust method that has been used for many years on Falcon aircraft. However, this reference method had to be enhanced to provide good estimations of flutter on T-tails. The first part of this paper presents T-tail flutter particularities and their consequences on flutter computations. It reads how the standard in-house DLM has been enhanced to account for in-plane motions of the HTP and fin bending. A first validation of this newly implemented tool is also presented in this section. It consists in the numerical restitution of a flutter test performed on a flexible T-tail mock-up at Mach 0.167. Enhanced DLM predictions are also compared with linearized RANS computations. To go further with the validation of flutter prediction using enhanced DLM and linearized RANS, a reference test in high subsonic and transonic domain was needed. The second part of this document reads how the CleanSky2 U-tail mock-up was reused and tested to capture the effect of the HTP lift and its dihedral angle on flutter. The last part focuses on the restitution of those T-tail effects exhibited during the tests performed at S2MA. Restitution is presented for both DLM and linearized RANS.

2 THEORETICAL BACKGROUND

2.1 Flutter Computations on T-tailed Aircraft and Methods

To study flutter, Equation 1 is fundamental. Written below in the Laplace domain with p the Laplace variable, it is usually solved in a reduced basis. In this equation, M, C and K are respectively the reduced mass, damping and stiffness matrices, GAF is the generalized aerodynamic force matrix, q is the dynamic pressure and X is the reduced coordinate vector. It is usually solved using a p-k solver that interpolates between unsteady GAF tabulated in the Mach number and k (the reduced frequency) in Equation 1. The unsteady GAF can be computed using any particular aerodynamic solver (DLM, linearized RANS, etc.).

$$[p^2M + pC + K - qGAF(Mach, k)]X = 0 \tag{1}$$

For T-tail applications, whatever the method, additional GAF have to be added to the one usually computed. Indeed in T-tail configurations the HTP placed on top of the fin tends to roll as the VTP bends. The steady airload then generates a side force as illustrated in Figure 1. Elastic deformations of the HTP will also contribute to this side force which is of prime importance when computing flutter on T-tailed aircraft. Those additional GAF are computed using a steady pressure flowfield and added to the regular unsteady GAF indifferently whether the unsteady GAF are derived from DLM or linearized RANS.

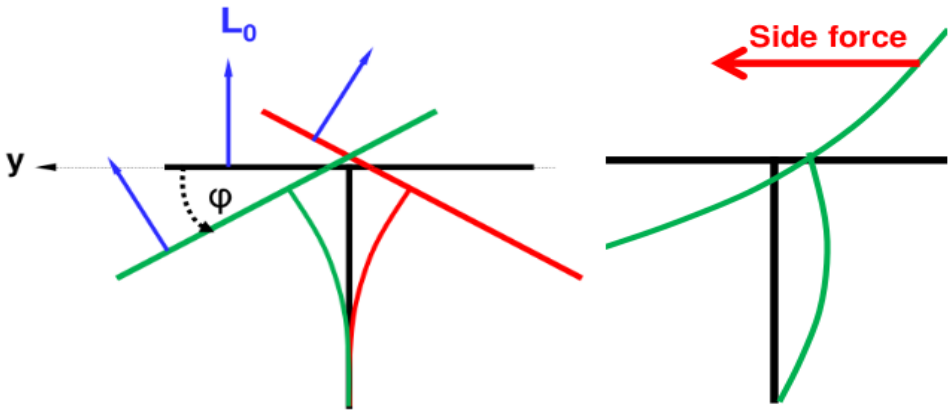

Figure 1 - Additional side force on T-tail configurations

2.1.1 Enhanced DLM Implementation at DASSAULT AVIATION

Standard DLM only takes into account heaving and pitching motions of the lifting surface. In-plane motions are usually neglected. This assumption works for the plane wings and for horizontal tails in classical cross tail configurations. However in a T-tail configuration, the HTP may exhibit significant roll, sideslip and in-plane motions as it moves along with the fin which is flexible. As seen before the effect of the roll motion is already taken into account indifferently depending on the aerodynamic method used (DLM or linearized RANS). In the case of computations performed with DLM, the code had to be enhanced to take into account the effect of sideslip and in-plane motions. The implementation performed is based on work by Queijo [3], Jennings [4] and van Zyl [5]. The additional effects added to the standard DLM in DASSAULT AVIATION tools are depicted in Figure 2 and can be summarized as follows:

- a sideslip effect that can be seen as a stiffness effect. The yawing motions generate a sideslip condition producing an additional lift on the fin which is computed based on the strip theory following Jennings and Queijo work.
- a lateral speed effect (y-wise motion). The sideslip angle due to a yaw displacement of the HTP is increased by the velocity in the y direction and leads to an additional lift on the fin. The effect is also called effective sideslip.
- a longitudinal speed effect (x-wise motion). This effect is also called effective windspeed. The x-deflections of the HTP change the velocity used in for computing the stagnation pressure with which the steady lift coefficient is normalized.

Those three effects corresponding to in-plane motions are naturally captured by linearized RANS methods. A first validation of the implementation was the comparison of resulting Fz, My and Mz obtained with enhanced DLM and linearized RANS computations. Comparisons have shown good agreement between both methods and it was possible to move forward with the code validation.

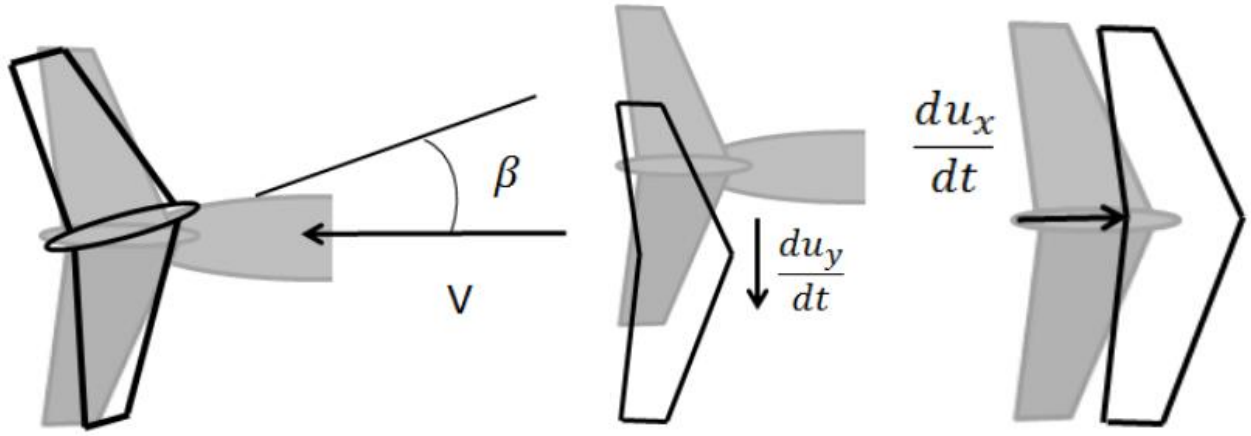

Figure 2 - Additional effects considered for T-tailed aircraft (from left to right: sideslip effect, lateral speed effect, longitudinal speed effect)

2.1.2 Linearized RANS Methods

A frequency-domain linearized Navier-Stokes solver taking into account linearized turbulence in a coupled form is used to predict unsteady aerodynamic forces. This linearized solver is integrated into the DASSAULT AVIATION in-house *AETHER* finite element flow solver. An efficient and highly scalable preconditioned GMRES solver is used to solve the resulting linear system [6].

2.2 Numerical Verification of T-tail Effects on Flutter in Subsonic Domain

To evaluate the accuracy of these newly implemented methods for flutter computations on intersecting surfaces, a restitution of Louw H. van Zyl wind tunnel experiment [5] was conducted. During these tests, a flexible T-tail mock-up was tested at Mach 0.167. Flutter speed was measured for different horizontal stabilizer angles of attack. The restitution was performed using both DLM and linearized RANS. The objective was to assess the ability of DASSAULT AVIATION in-house codes to predict flutter speed taking into account the particular effects of a T-tail.

On a structural point of view, a reduced model was created using data provided in [5] on the structural modes, the flutter equation being solved in a reduced modal basis. Steady and unsteady aerodynamic forces were then computed using either linearized RANS or enhanced DLM. For CFD computations, a mesh was generated based on a SolidWorks model provided by L. H. van Zyl (Figure 3). DASSAULT AVIATION in-house linearized RANS code *AETHER* was used to performed both steady and unsteady computations.

Figure 4 presents the results obtained with enhanced DLM. The evolution of flutter speed with the horizontal stabilizer angle of attack is well predicted with enhanced DLM. An offset is noticed between experimental data and numerical prediction. However this offset is not due to the additional terms implemented in the enhanced DLM as the classical DLM also presents this discrepancy for the horizontal stabilizer at an angle of attack of 0° where the HTP lift is equal to zero. The dotted line in Figure 4 shows that with a correction of this offset, the effect of the HTP lift is really well predicted, the line being really close to the experimental values.

These results were then compared with linearized RANS computations. Results obtained with DASSAULT AVIATION in-house solver *AETHER* are closer to the experimental data in

comparison with enhanced DLM as depicted in Figure 5. A deeper investigation has shown that the aerodynamics forces computed with both methods differ in the obus region (junction between the fin and the horizontal tail plane). The simplified modelling of this region on the DLM mesh leads to small discrepancies on the aerodynamic fields computed in that zone. This zone moves in the flexion mode shape leading to differences on the aerodynamic forces computed and ultimately on the flutter speed.

Figure 3 - Surface mesh for CFD analysis

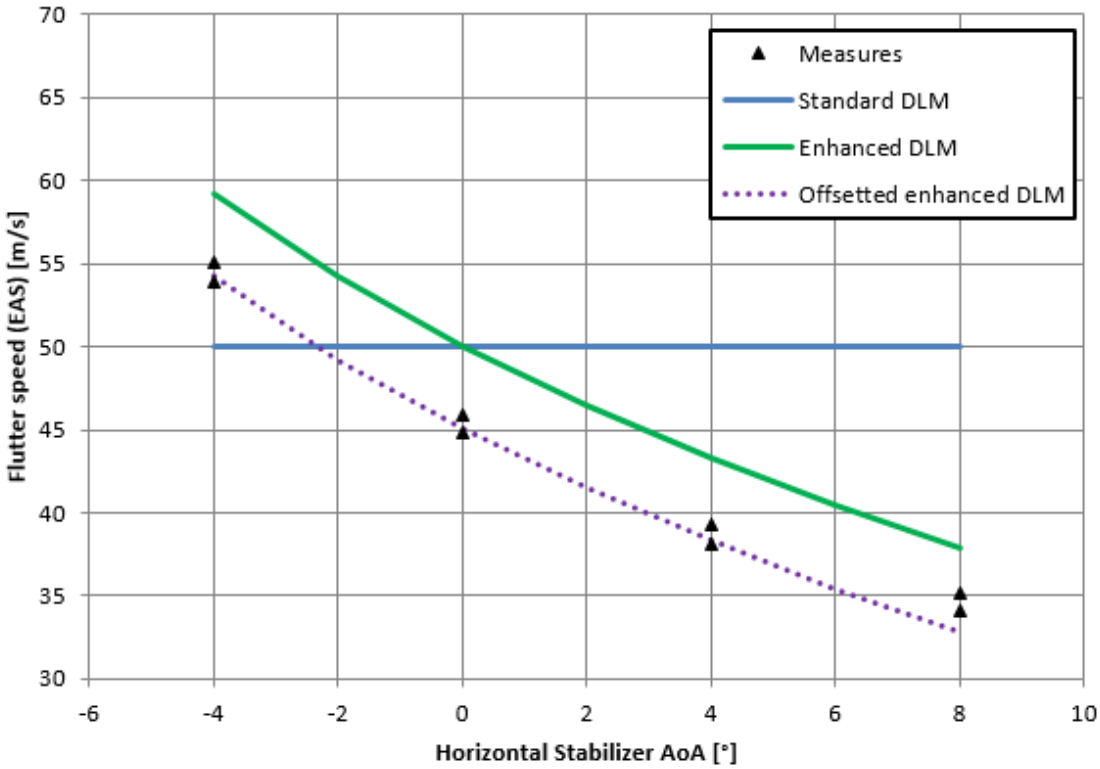

Figure 4 - Flutter prediction correlation with measurements on van Zyl T-tail mock-up

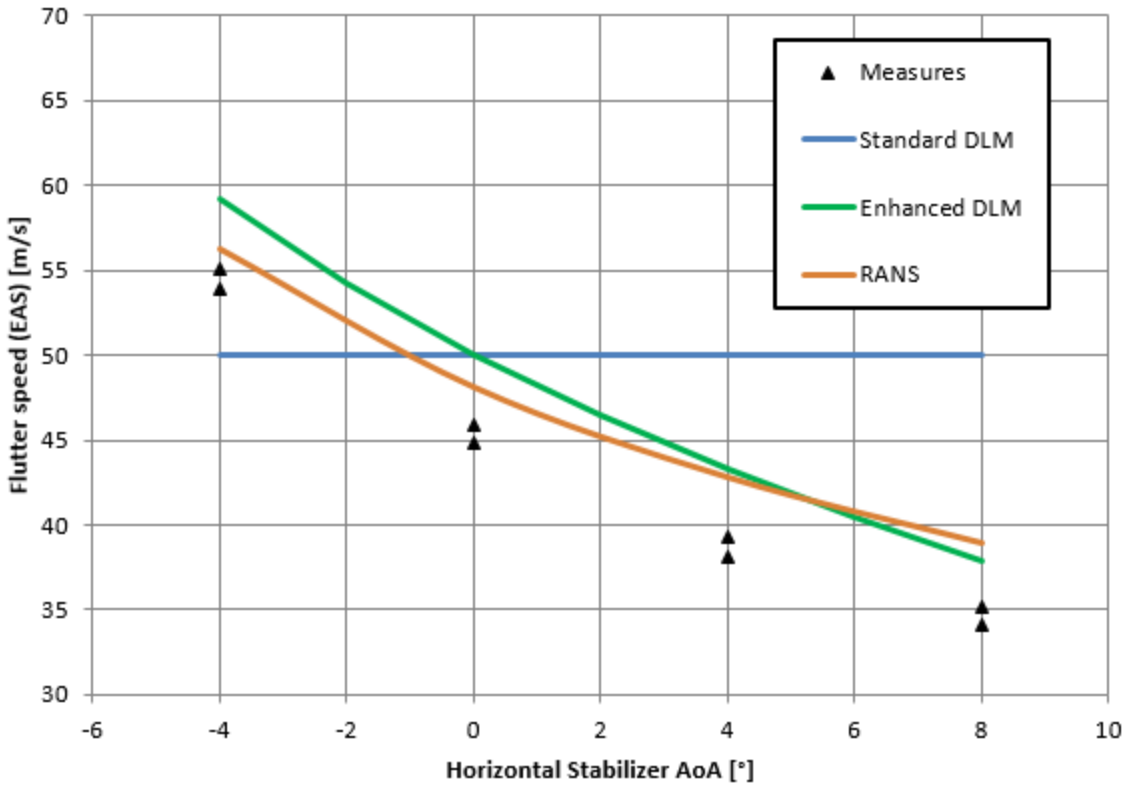

Figure 5 - Flutter prediction comparison between linearized RANS and DLM

This numerical verification work constituted a first validation of the DASSAULT AVIATION in-house solvers. The implemented enhanced Doublet Lattice Method and the *AETHER* solver both allow an accurate prediction of flutter speed accounting for particular phenomena T-tail configurations. However L. H. van Zyl tests were only performed at Mach 0.167. The validation of the implementation of enhanced DLM was thus incomplete with no validation in high subsonic and transonic domains. It was decided to perform wind tunnel tests at higher Mach numbers in cooperation with ONERA.

3 T-TAIL FLUTTER MOCK-UP FOR HIGH SUBSONIC AND TRANSONIC WIND TUNNEL TESTING

3.1 Mock-up Presentation

A wind tunnel test mock-up has been designed and manufactured in the frame of CleanSky2 project NACOR in cooperation between DASSAULT AVIATION, ONERA and RUAG. This mock-up was tested in 2016 for U-tail configurations [1]. Its design is extensively presented in [7]. A brief summary is presented herebelow.

The mock-up was designed to study a flutter mechanism involving bending and torsion modes of the fin. The general architecture is depicted in Figure 6. The main difference with L. H. van Zyl mock-up is that in-wind parts are here rigid. The in-wind parts are linked to a shaft which is connected to a table by two bearings and a long straight beam. With this architecture a torsion of the fin (referred to as HTP in figure and in the rest of this article) correspond to a pitch motion around the shaft. The frequency of this pitch mode is directly driven by the straight beam stiffness.

Similarly, the fin bending corresponds to a roll mode of the mock-up as the table is linked to the wall by two bearings and several S-shaped spring beams. The roll stiffness could easily be adjusted with the number of S-beams whose stiffness was directly driving the mode frequency.

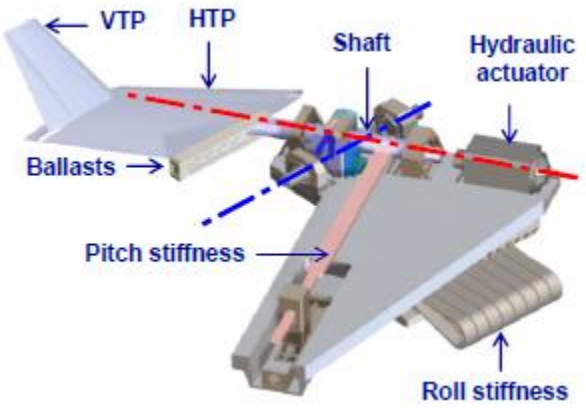

Figure 6 - General view of the mock-up

With this ability to change pitch stiffness (by varying the length of the straight beam) and the roll stiffness, as well as the possibility to add ballast, modifications of the mock-up could be envisioned. Indeed, with all these adjustments parameters it was easy to convert this U-tail into a T-tail while keeping its dynamic behavior. Tests performed in 2016 have shown that the dynamic behavior of the mock-up was excellent [1] and perfectly fitted for the S2MA wind tunnel pressure variations with observable flutter onset from subsonic to transonic Mach numbers. On this mock-up the safety system consisted in an hydraulic actuator blocking the shaft when dedicated accelerometers threshold were exceeded. For more details see [7].

To evaluate the enhanced DLM code several VTP settings had to be tested. To do so the tip of the fin was modified. With a set of different adapters (as depicted in Figure 7), it was possible to change quickly from one setting to another. Three VTP settings (-4°, -2°, +1°) were designed to be tested as they would permit to acquire data on the effect of the VTP lift on flutter. An extra setting with a dihedral angle (-10°) was also tested. Figure 8 recalls the angle definitions used in this article. It is worth mentioning that the -2° VTP setting corresponds to a configuration with a VTP lift coefficient close to zero, while the +1° setting and the -4° setting correspond respectively to a negative lift coefficient and a positive one.

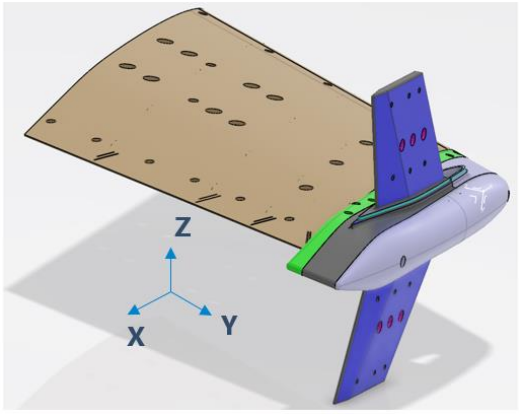

Figure 7 - New adapters for T-tail configurations

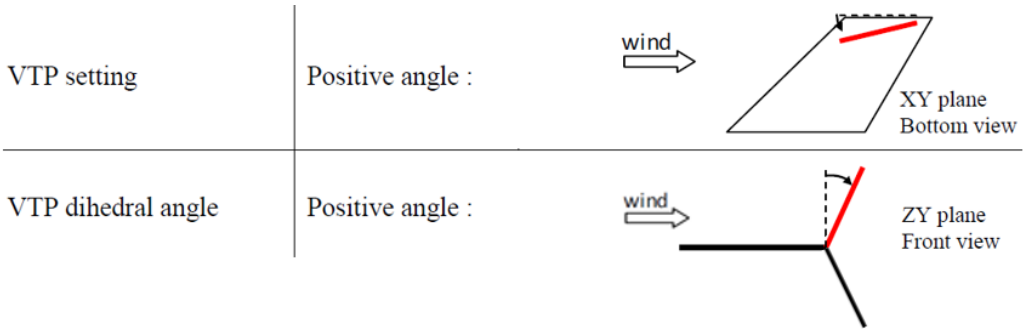

Figure 8 - Angles definition

The instrumentation of the mock-up included accelerometers and pressure sensors in both upper and lower VTP in addition to the ones present in the 2016 mock-up. In total the mock-up was instrumented with 259 pressure sensors and 45 accelerometers as depicted respectively in Figure 9 and Figure 10.

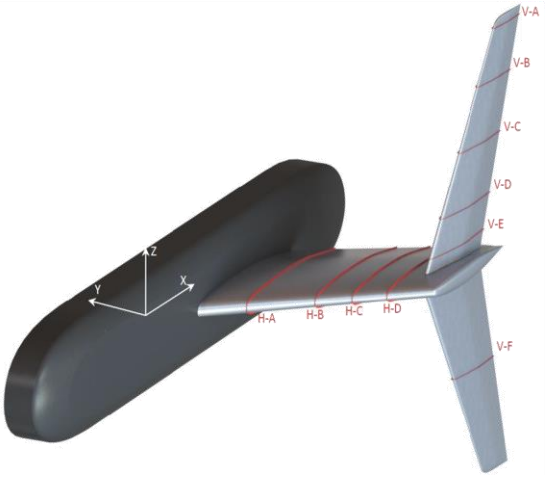

Figure 9 - Pressure sensors locations

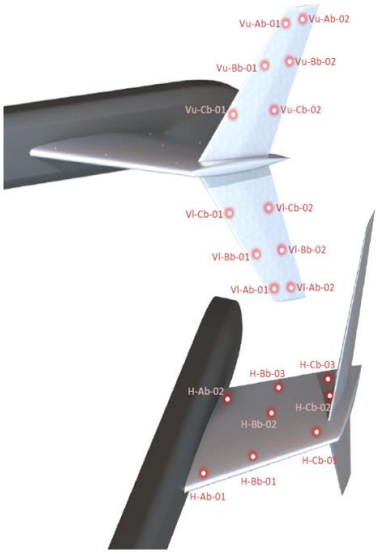

Figure 10 - Accelerometers locations

3.2 Lessons Learnt and Improvements on the Mock-up

During the previous test campaign in 2016 some discrepancies were observed on flutter onset repeatability. In preparation for a second wind tunnel test campaign, a closer look was taken at the local flow separation observed at the fin root at the 2016 campaign. As illustrated in Figure 11, in steady flow conditions in the wind tunnel, a separation was observed. It was the consequence of a leakage through the opening in the wind tunnel wall. This leakage was due to the pressure difference between inside and outside the wind tunnel vane. Some tests were performed to assess the impact of this separation using scotch tape to seal the opening in the wall (Figure 12). The impact of this leakage can be seen on the unsteady pressure coefficients measured at the fin root as illustrated in Figure 13 and Figure 14. These unsteady pressure coefficients were measured for a harmonic pitching motion of the mock-up around its shaft. It was not possible to use the tape during flutter test as it would change the mock-up stiffness and get completely torn during diverging oscillations.

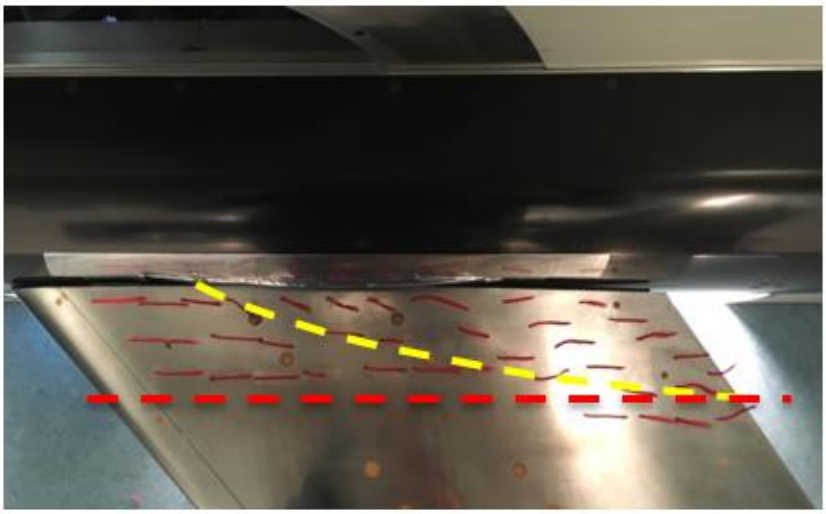

Figure 11 - Local separation at fin root. Kulites cut H-A is represented by the red dotted line

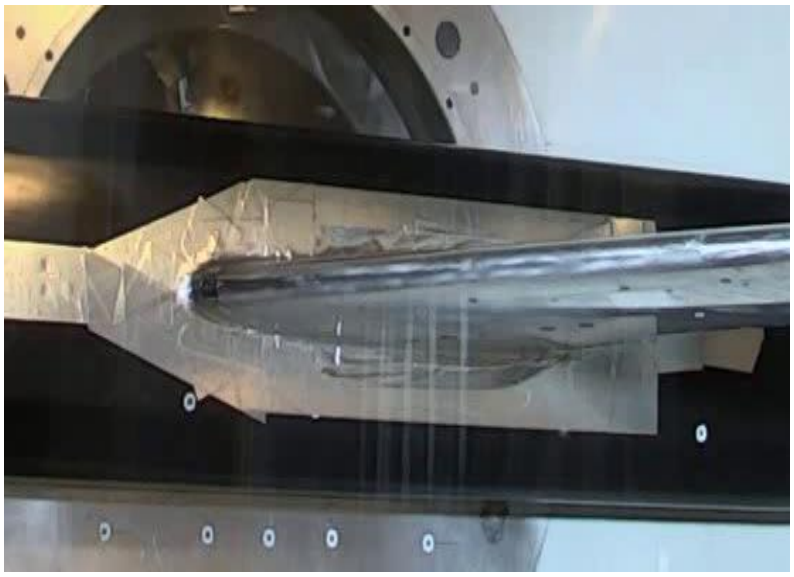

Figure 12 - Tape sealing of the fuselage opening

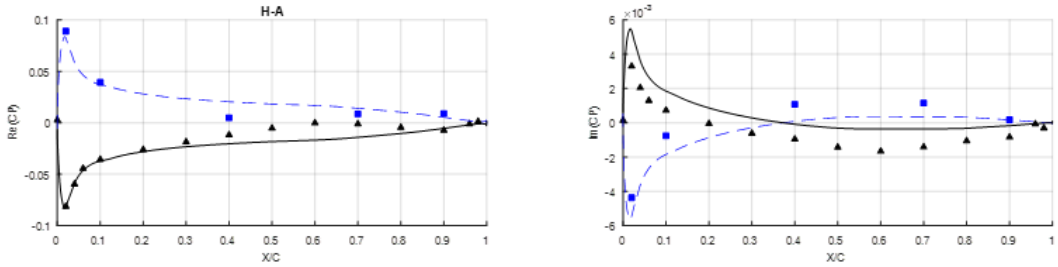

Figure 13 - Comparison between numerical prediction (lines) and experimental data (markers) without tape sealing

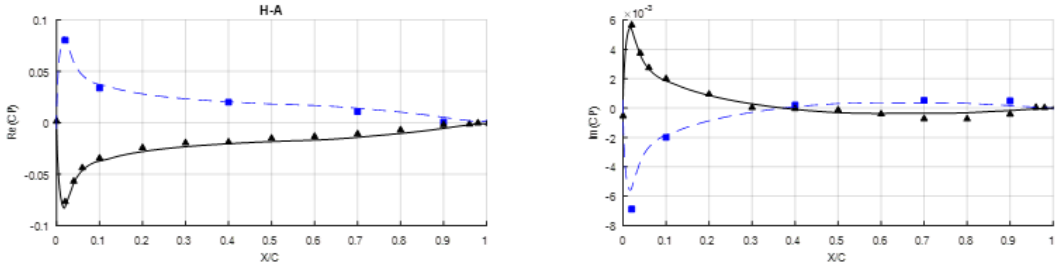

Figure 14 - Comparison between numerical prediction (lines) and experimental data (markers) with tape sealing

This leakage is deemed to be the cause of the discrepancies observed during the restitution of the previous 2016 campaign and the imperfect repeatability of flutter onsets. To improve this behavior, studies were performed in 2021 in collaboration between ONERA and DASSAULT AVIATION. They led to the development of a sealing system using labyrinths to reduce air leakage. The sealing system is presented in details in paper IFASD-2024-165 [8].

3.3 Wind Tunnel Test Plan

The objective of this new wind tunnel test campaign being the validation of enhanced DLM, it was decided to test the different VTP testing at Mach numbers ranging from 0.7 to 0.925. The campaign consisted of three different tests: ground vibration tests, pressure tests and flutter tests. Ground vibration tests are important for structural correlation. Due to the modifications on the mock-up, it was important to get data to tune the new finite element model of the mock-up. The so-called pressure tests are of prime interest for aerodynamic correlation. During pressure test, harmonic pitching oscillations are applied to the mock-up around its shaft. Steady and unsteady pressure data are measured during these tests for several Mach numbers and pitching frequencies. Finally, flutter tests are conducted to generate flutter curves for several Mach numbers up to the flutter point. The following section will present the results obtained for all types of test and their correlation with numerical predictions.

Figure 15 - T-tail mock-up installed in S2MA wind tunnel

4 NUMERICAL RESTITUTION OF WIND TUNNEL TEST CAMPAIGN

4.1 Ground Vibration Tests and Finite Element Model Updating

When building a flutter diagram, ground vibration tests (GVT) give the first point on the flutter curve at zero-speed condition. It is of prime importance to have a correct identification of the structural modes wind-off to calibrate the finite element model and perform accurate flutter computations. It is also important to perform GVT regularly during the test campaign to check that the dynamic behavior of the mock-up does not change during the campaign. A change in the dynamic response could indicate structural damage especially if flutter onset is approached or exceeded.

GVT were performed regularly during the test campaign and have shown good repeatability. Modal analysis was conducted using DASSAULT AVIATION in-house tool ALAMO [9]. The finite element model was then locally tuned to be representative of the measured mock-up dynamic behavior. Special care was put on matching the modal properties of the first two structural modes (bending and torsion) as they are the ones coupling in the flutter mechanism. A good correlation was obtained as illustrated in Figure 16 and Figure 17. These figures show that computed frequency response functions match the measured ones for the corresponding sensors on the mock-up. Finally, Figure 18 shows that the modal shapes computed are very close to the measured ones since the modal assurance criterion (MAC) matrix is close to identity.

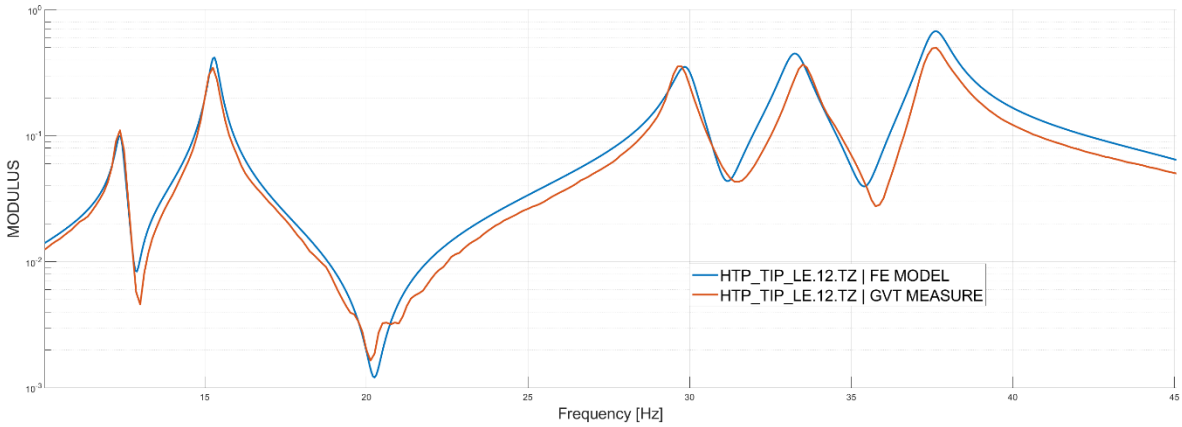

Figure 16 - Comparison between computed and measured frequency response functions for an HTP sensor

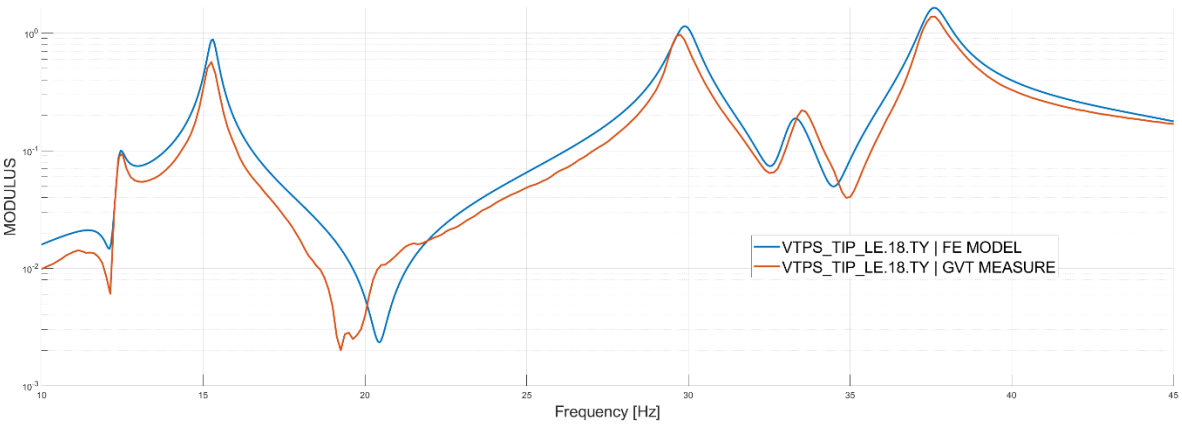

Figure 17 - Comparison between computed and measured frequency response functions for a VTP sensor

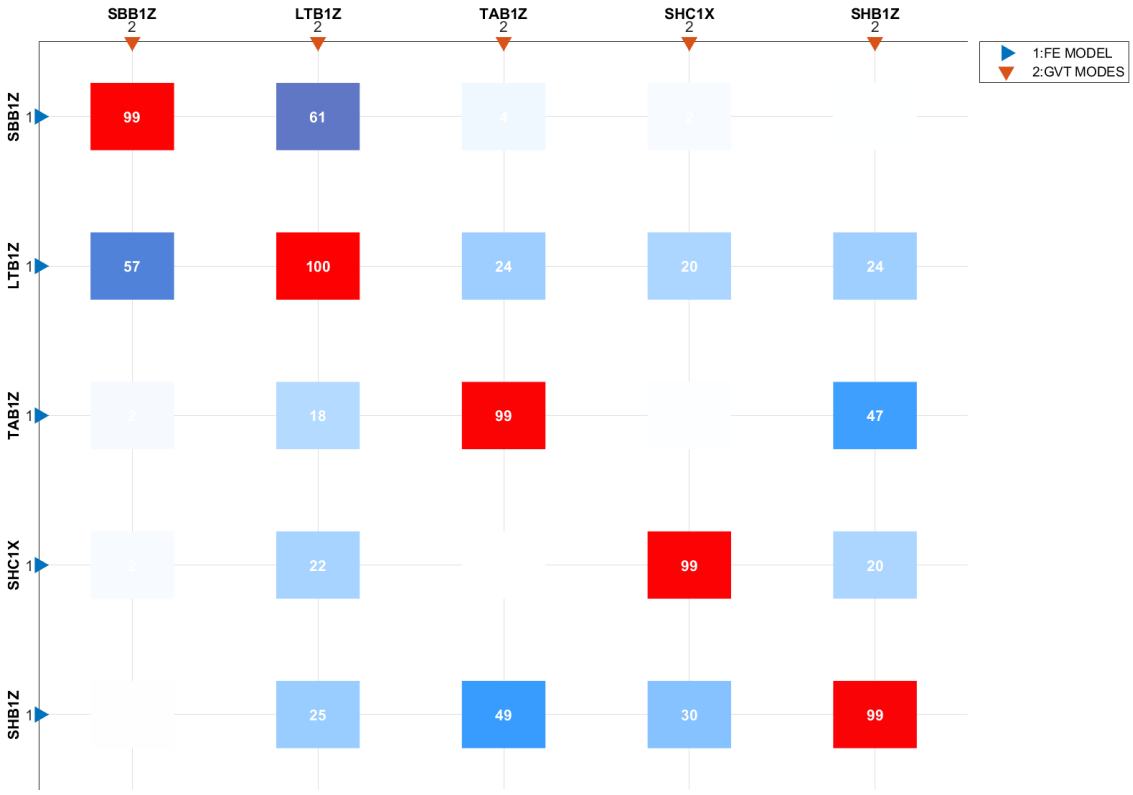

Figure 18 - Cross MAC matrix between computed and measured modes

Having an adequate structural correlation, it is possible to move further with flutter correlations and focus on the effect of aerodynamics on the structure.

4.2 CFD Restitution of Pressure Tests

The first part of the campaign was devoted to pressure tests (pressure configuration). The principle of these tests is to apply harmonic oscillations to the mock-up (HTP+VTP) for different Mach numbers, angles of attack, frequencies and forcing amplitudes. Three cases have been investigated corresponding to different flow regimes encountered by an aircraft: subsonic (M = 0.70), transonic (M = 0.875) and high transonic regime (M = 0.925).

4.2.1 Steady pressure coefficients

4.2.1.1 Geometrical effect

A geometric sensitivity test was carried out to assess whether it was necessary to take into account the gap between the HTP and the fuselage and/or to include the HTP axis. Three geometries were generated and numerically assessed by CFD: “no gap” (reference, n°1), “with gap” (n°2) and “with gap and axis” (simplified HTP axis, n°3), see Figure 19.

Results are presented for three cuts: cuts H-D and V-E are located close to the HTP/VTP junction respectively on the HTP and VTP parts. Cut V-C is located close to the middle of the VTP (see Figure 9). As shown in Figure 20, no geometrical effect is observed for the subsonic regime (M = 0.7) and a very good correlation between CFD and wind tunnel test (WTT) results is achieved.

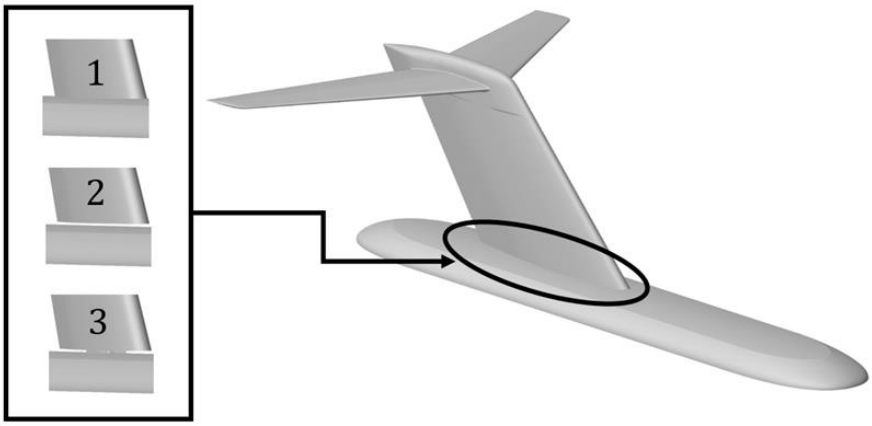

Figure 19 - Geometrical effect: Fuselage/HTP junction

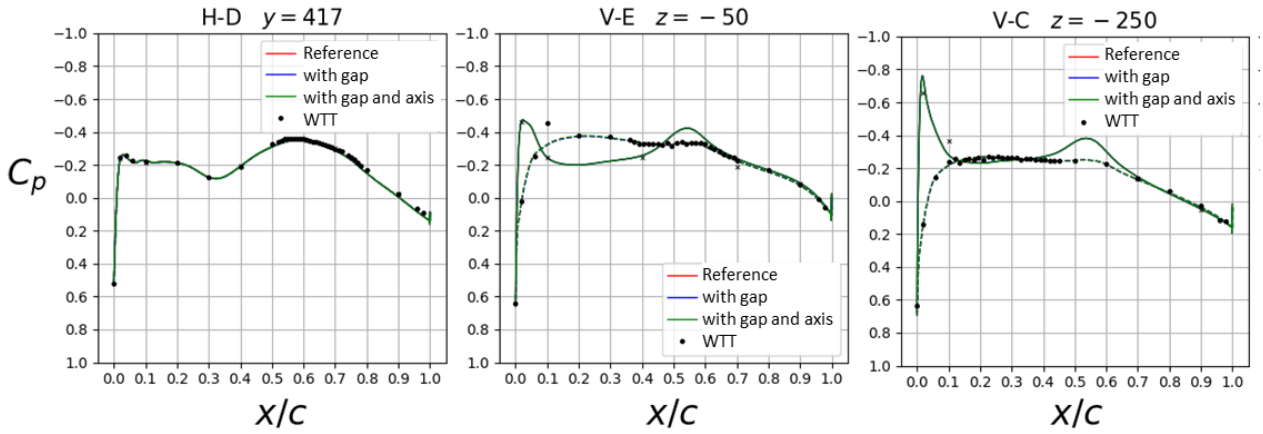

Figure 20 - Geometrical effect: Cp distribution for -2° VTP setting in subsonic regime (M = 0.7)

Results for M = 0.875 are presented in Figure 21. No geometrical effect is observed for this Mach number. Nevertheless, the shock location is not well predicted by CFD whatever the fuselage/HTP junction.

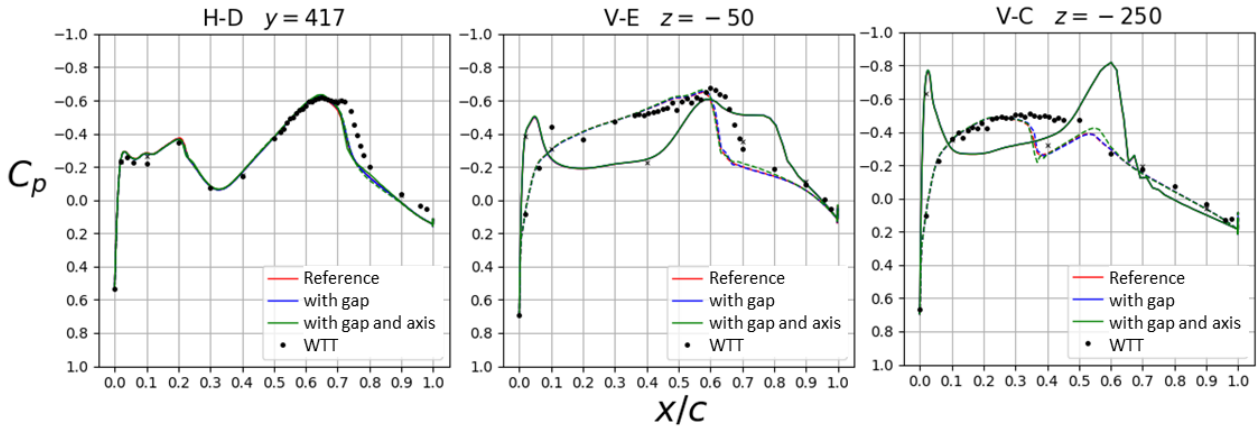

Figure 21 - Geometrical effect: Cp distribution for -2° VTP setting in transonic regime (M = 0.875)

For high transonic regime (M = 0.925), results are presented in Figure 22: the shock location predicted by CFD is too upstream with a flow acceleration in the shock region that is not present in the WTT results. The supersonic region upstream of the shock is overestimated by CFD computations. Slight differences are observed for the "gap and axis" case (H-D and V-E cuts) but it does not improve the correlation between CFD predictions and WTT results.

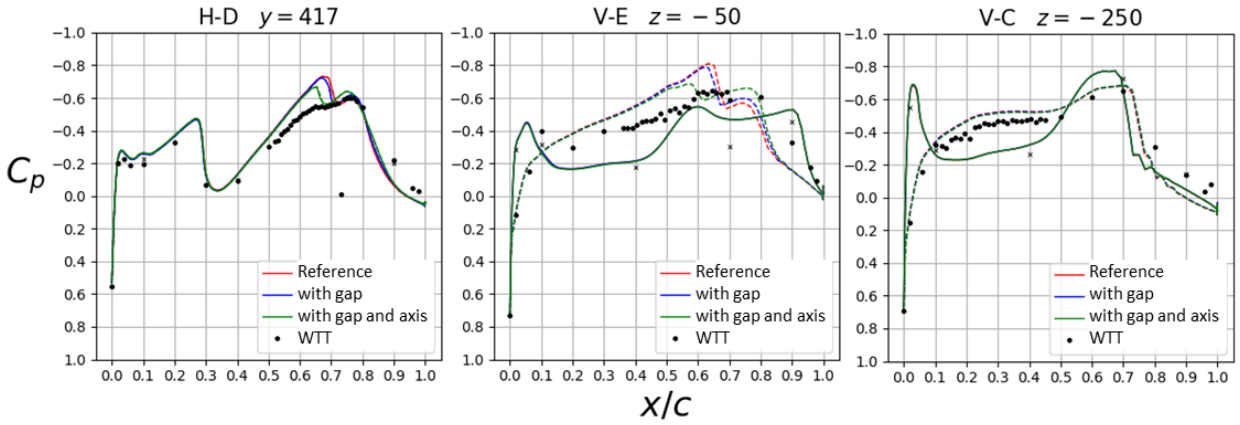

Figure 22 - Geometrical effect: Cp distribution for -2° VTP setting in high transonic regime (M = 0.925)

4.2.1.2 VTP setting effect

The VTP setting effect for the subsonic regime is presented in Figure 23. The "with gap"-configuration is the only configuration considered for this assessment. A very good correlation is obtained for all VTP settings in subsonic regime.

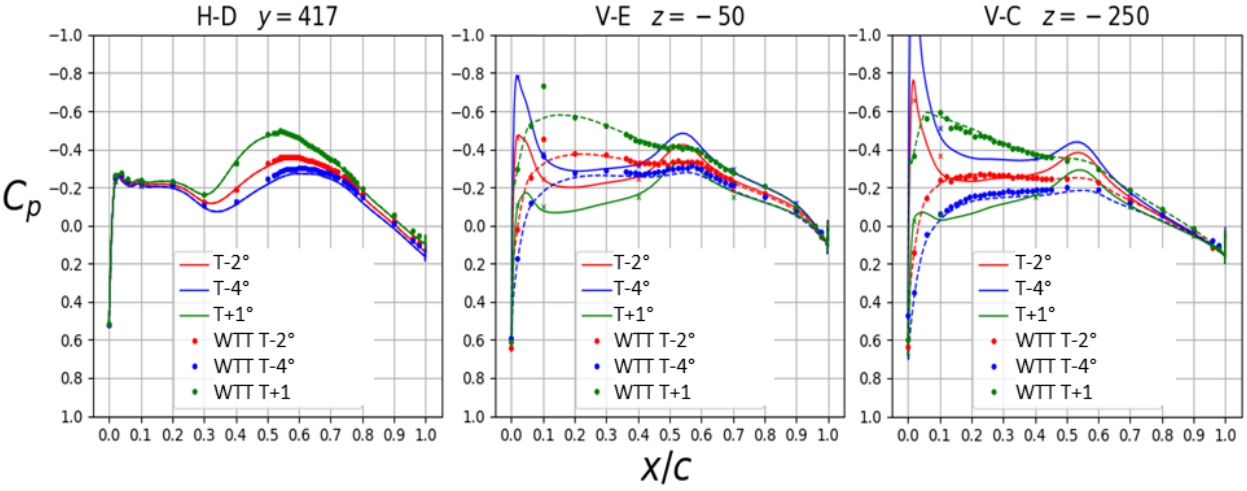

Figure 23 - VTP setting effect: Cp distribution for the different VTP settings in subsonic regime (M = 0.70)

For the transonic regime (M = 0.875), the best prediction of the shock location is obtained with the +1° VTP setting. For -2° VTP and -4° VTP settings, the shock predicted by CFD is located upstream of the WTT shock location and the greater the absolute value of the VTP setting, the greater the difference between CFD computation and WTT results.

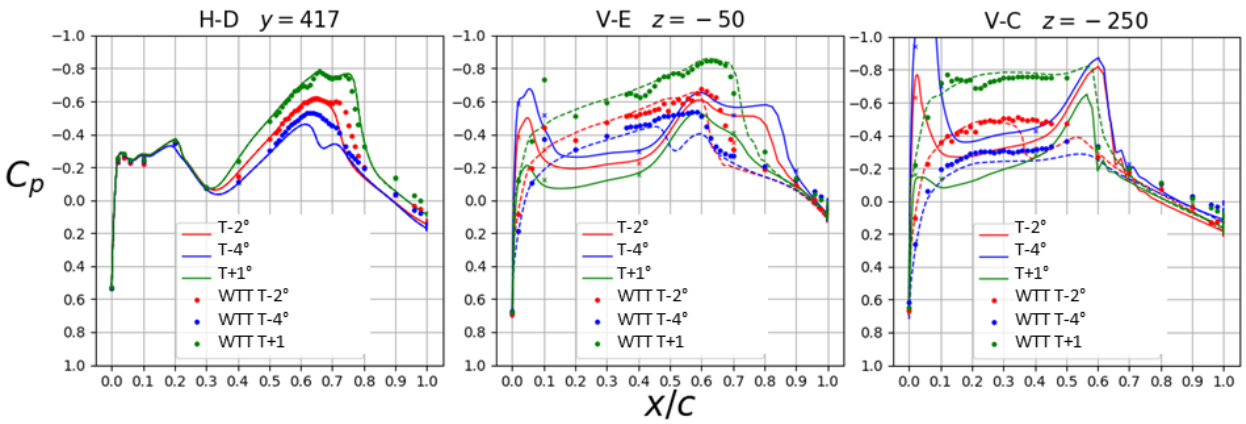

Figure 24 - VTP setting effect: Cp distribution for the different VTP settings in transonic regime (M = 0.875)

For the high transonic regime (M = 0.925), upstream of the shock, the CFD Cp-distribution is overestimated on both HTP & VTP for +1° and -2° VTP settings. A better correlation is observed for the Cp-distribution in this region with the -4° VTP setting (cut V-C). Nevertheless the shock location remains offsetted from the one observed in WTT.

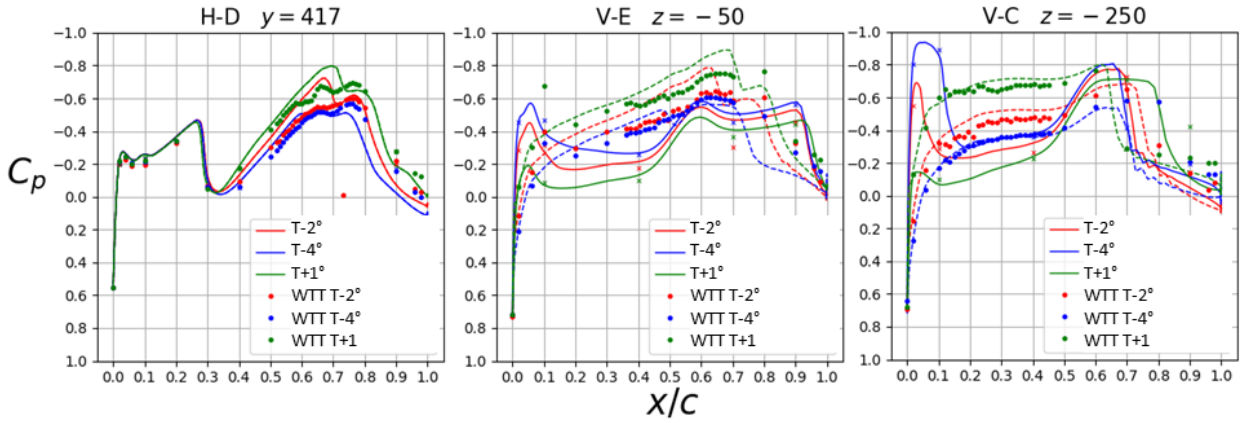

Figure 25 – VTP setting effect: Cp distribution for the different VTP settings in high transonic regime (M = 0.925)

4.2.2 Unsteady pressure coefficients

Quasi-steady and unsteady pressure coefficients variations are presented for different geometric effects corresponding to a mock-up angle of attack (AoA) amplitude of +/-0.2°: the reference configuration without gap between fuselage and HTP, the “with gap” configuration with the 5 mm gap present on the mock-up and the “with gap and axis” configuration with the 5 mm gap and a generic geometry for the HTP axis. Only the -2° VTP setting is presented in this section. Similar results are obtained for the other VTP settings.

4.2.2.1 Geometrical effect

4.2.2.1.1 Quasi-steady (f = 0 Hz)

Quasi-steady pressure coefficients are plotted at M = 0.7 (Figure 26). For this Mach number, the unsteady CFD predictions are improved by the presence of the gap for both HTP&VTP distributions.

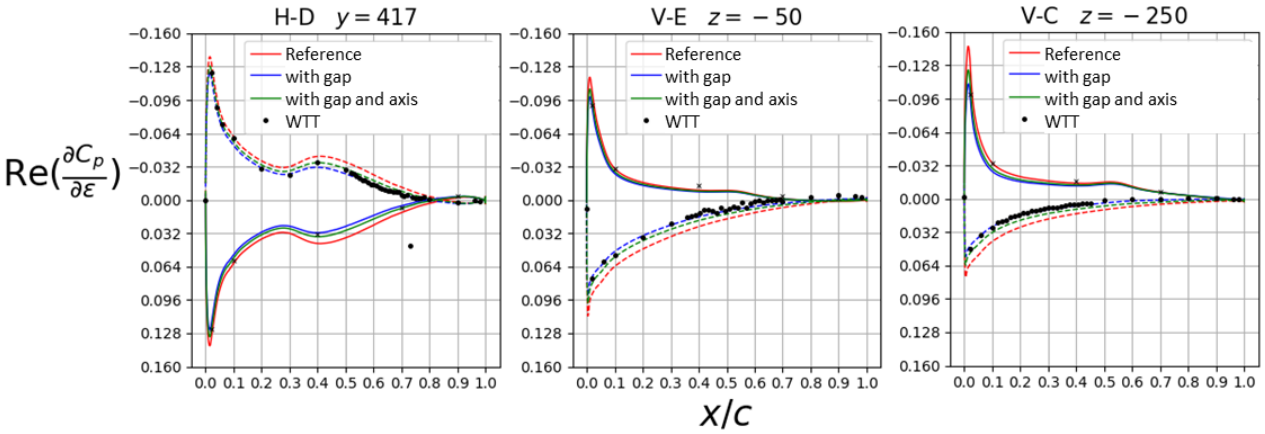

Figure 26 - Geometrical effect: Re(∂Cp/∂ε) distribution for -2° VTP setting in subsonic regime (M = 0.7)

This result is confirmed for the transonic regime (M = 0.875, Figure 27) with a very good prediction of the unsteady pressure coefficients near the shock area in the HTP&VTP junction (0.6 < x/c < 0.7) and an overestimation of these coefficients for the reference configuration.

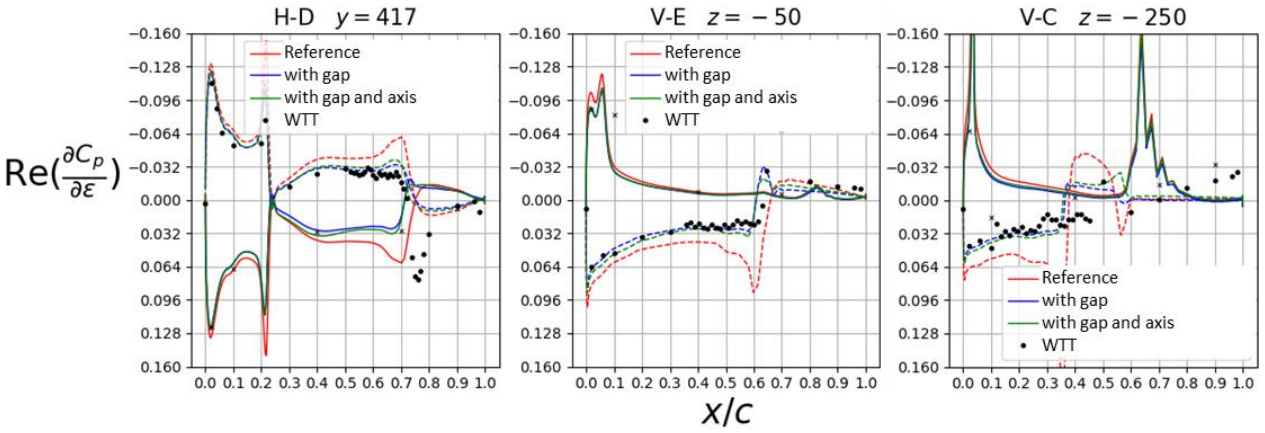

Figure 27 - Geometrical effect: Re(∂Cp/∂ε) distribution for -2° VTP setting in transonic regime (M = 0.875)

For high transonic regime, the multiple shock occurrence makes it difficult to analyze the differences between CFD and WTT results. Nevertheless, the pressure load upstream of the rear shock seems to be better predicted when the gap is taken into account, especially on the VTP.

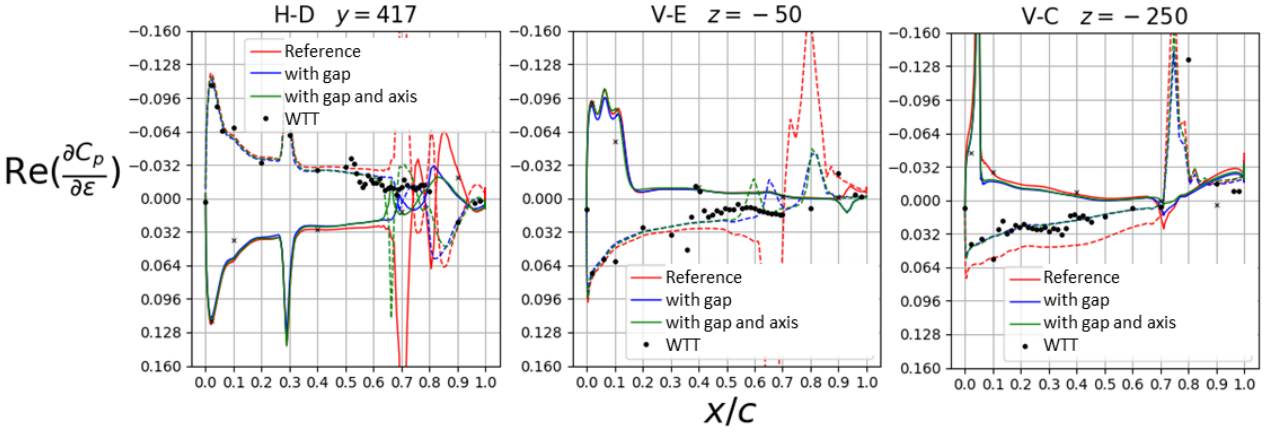

Figure 28 - Geometrical effect: Re(∂Cp/∂ε) distribution for -2° VTP setting in high transonic regime (M = 0.925)

4.2.2.1.2 Unsteady – f = 5 Hz

The first flow condition addressed for this test case is Mach 0.7 and for different geometric effects: reference configuration without gap between fuselage and HTP, the "with gap" configuration with the 5 mm gap present on the mock-up and the "with gap and axis" configuration with the 5 mm gap and a generic geometry for the HTP axis. In Figure 29 are illustrated both real and imaginary parts of unsteady pressure coefficient distributions. At this Mach number, the flow is shock-less on the HTP/VTP configuration. In the top part of the figure is presented the real part of the unsteady pressure coefficients induced by a harmonic motion at 5 Hz and an AoA amplitude of +/-0.2°. In the lower part of the figure is presented the imaginary part of the unsteady pressure coefficients induced by the harmonic motion. The best CFD-WTT correlation is obtained with the "with gap" configuration.

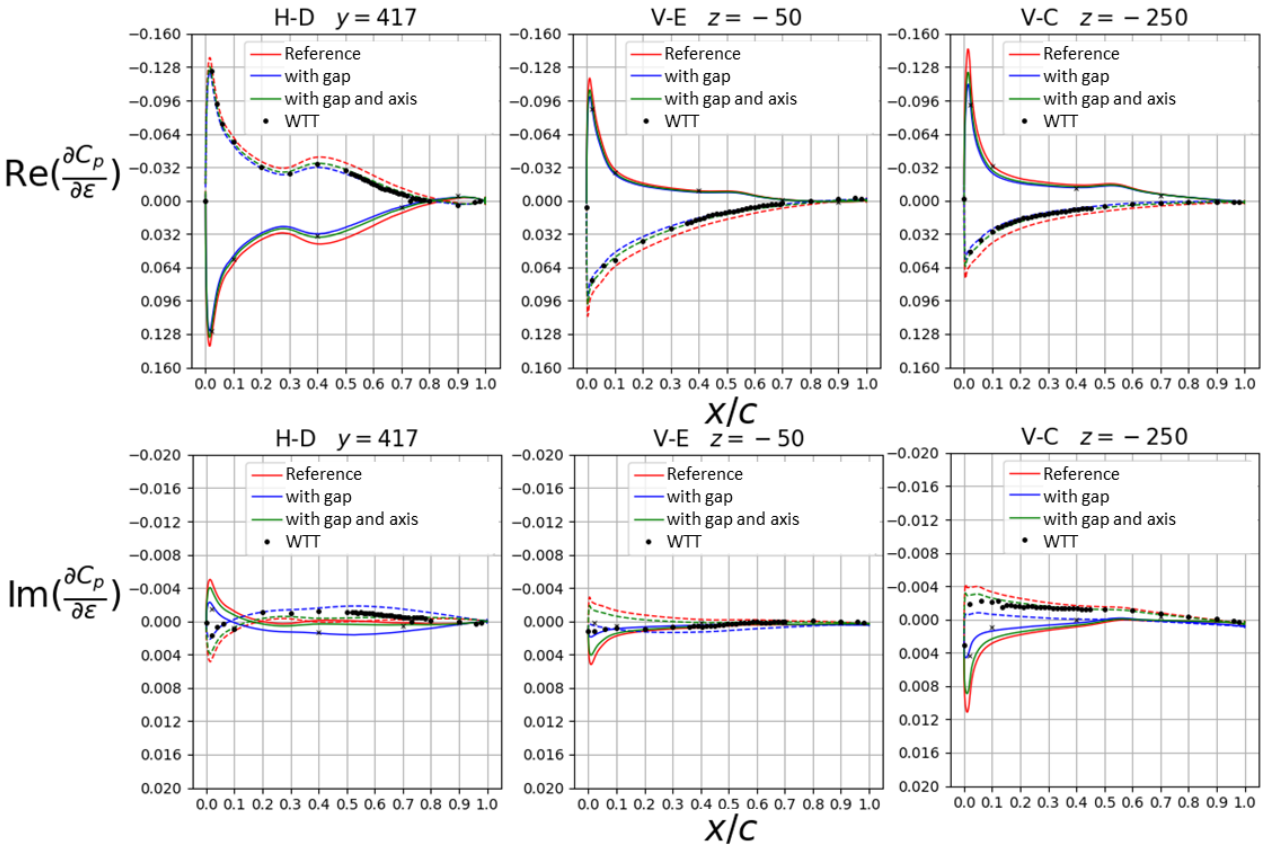

Figure 29 - Geometrical effect: Re(∂Cp/∂ε) and Im(∂Cp/∂ε) distribution for -2° VTP setting in subsonic regime (M = 0.7)

The second flow condition addressed on this test case is the transonic regime, i.e. Mach = 0.875. In Figure 30 are illustrated both real and imaginary parts of the unsteady pressure coefficient distributions for f = 5 Hz and an AoA amplitude of +/-0.2°. For the real part (top part of the figure), the correlation between CFD and WTT is satisfactory in the junction area (cuts H-D and V-E) with the "with gap" configuration (with or without axis) unlike the reference configuration. For the imaginary part (lower part of the figure), taking into account the gap improves the pressure loading variation upstream of the shock. However, the shock motion is not well predicted and actually depends on the presence of the HTP axis in the computation.

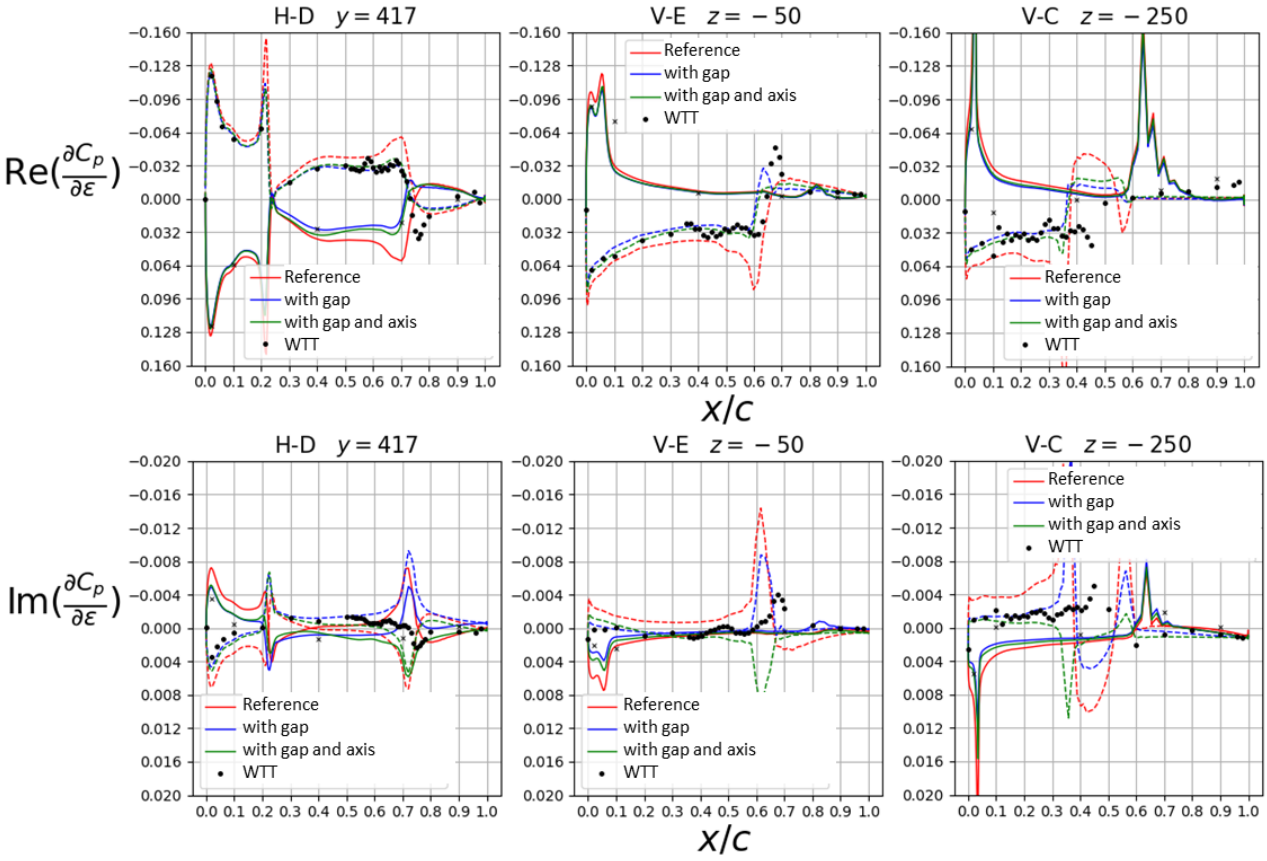

Figure 30 - Geometrical effect: Re(∂Cp/∂ε) and Im(∂Cp/∂ε) distribution for -2° VTP setting in transonic regime (M = 0.875)

For the high transonic regime, i.e. Mach = 0.925, both real and imaginary parts of unsteady pressure coefficient distributions are shown in Figure 31 for f = 5 Hz and an AoA amplitude of +/- 0.2°. For the real part (top part of the figure), the conclusion is the same as for the f = 0 Hz case (see 4.2.2.1.1): there is no correlation between CFD prediction and WTT results for the shock displacement in the junction area but a better prediction of the unsteady load upstream of the shock when a gap is present in the simulation (with or without axis). For the imaginary part (lower part of the figure), the conclusion is similar.

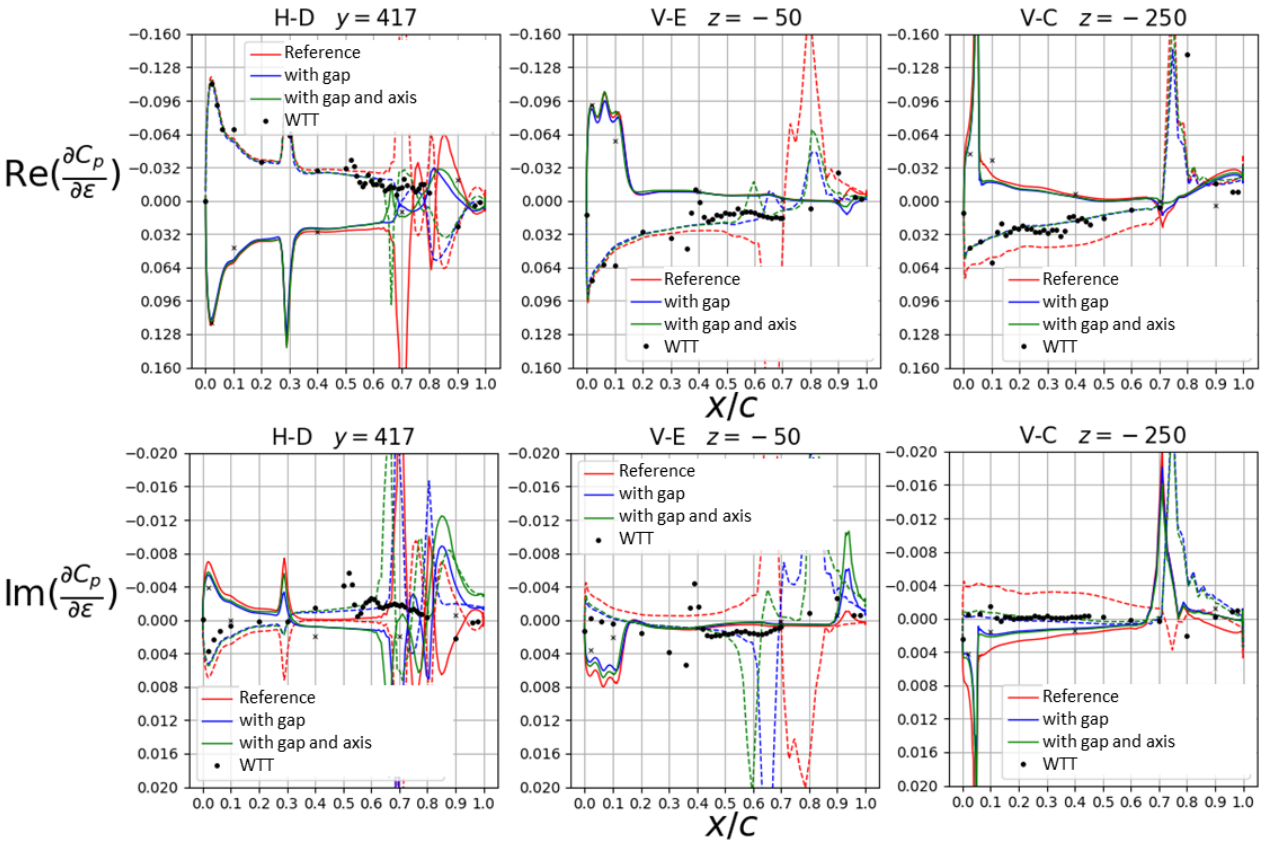

Figure 31 *- Geometrical effect: Re(∂Cp/∂ε) and Im(∂Cp/∂ε) distribution for -2° VTP setting in high transonic regime (M = 0.925)*

4.2.3 Synthesis

CFD restitution of the pressure tests indicates that the best correlation with WTT results is obtained for the "gap" configuration (taking into account the 5 mm gap). The axis modelling does not improve the correlation, mainly due to difficulties in converging the linear system (blunt axis generating a separated flow wake). A less intrusive geometric modelling of the axis could improve the linear system convergence. For the "gap" configuration, unsteady loads are more coherent with the experimental data, especially the real part of the unsteady loads whatever the Mach number considered. Discrepancies remain for the imaginary part of the unsteady loads and a sensitivity to the reference phase applied to the experimental data to determine the imaginary part is still in progress. Flutter test restitutions hereafter are obtained with linearized RANS computations performed on the "gap" configuration.

4.3 Flutter Tests Restitution

4.3.1 Flutter Prediction Correlations with Measurements

Having adequate structural and aerodynamics correlations, flutter restitution can provide an assessment of the flutter solvers.

Flutter diagrams represent the in-wind evolution of the modes frequency and damping up to flutter onset. The abscissa used for the flutter diagrams in this article is the wind tunnel total pressure. Indeed, the ONERA S2MA wind tunnel is pressurized so it was possible to increase the total

pressure at a fixed Mach number. Modal frequencies and damping at a zero total pressure are extracted from the GVT data. Vibration tests were also performed for several stagnation pressures at a fixed Mach number to evaluate the evolution of the modal characteristics with flow conditions. Random white noise excitations were applied using the mock-up actuator, the accelerometers time data were then post-processed and modal analysis was performed with the same tools and procedure as the GVT. Finally, to obtain the flutter onset pressure value, a special post-processing has been applied as presented in [1]. After increasing the wind tunnel total pressure and performing several in-wind vibration tests, the total pressure in the wind tunnel is increased continuously until flutter onset. Numerical predictions were used to get a first estimation of the critical flutter pressure and then, starting from a slightly lower total pressure, the wind tunnel pressure was increased. Time data around flutter onset are curve-fitted following Equation 2 and as illustrated in Figure 32 to get flutter characteristics: frequency ω, damping ξ and shape A and φ.

$$s(t) = A\, e^{-\xi\omega t} \sin(\omega t + \varphi) \tag{2}$$

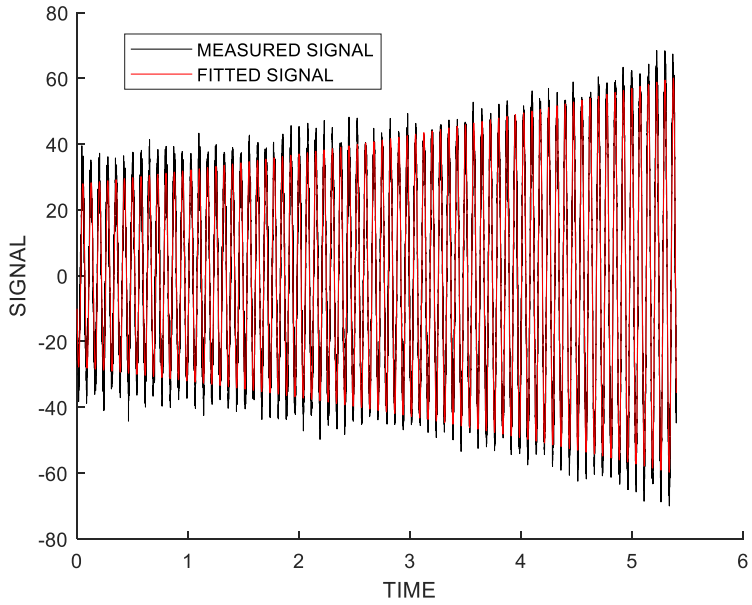

Figure 32 - Curve fitting of time data at flutter onset

Following this post-processing procedure, experimental flutter curves were built and compared to numerical predictions. Figure 33 shows an example of the correlation obtained for the -2° VTP setting with enhanced DLM. The flutter critical pressure is also well predicted for all Mach number with slight discrepancies observed above Mach 0.875. These discrepancies are explained by transonic phenomena that the enhanced DLM is not meant to predict.

Figure 33 also presents a synthesis of the results obtained using both linearized RANS and enhanced DLM methods. Excellent agreement is observed between experimental data and numerical predictions. As already noted, enhanced DLM shows its limits for high transonic Mach numbers in the particular case of this T-tail mock-up but remains conservative.

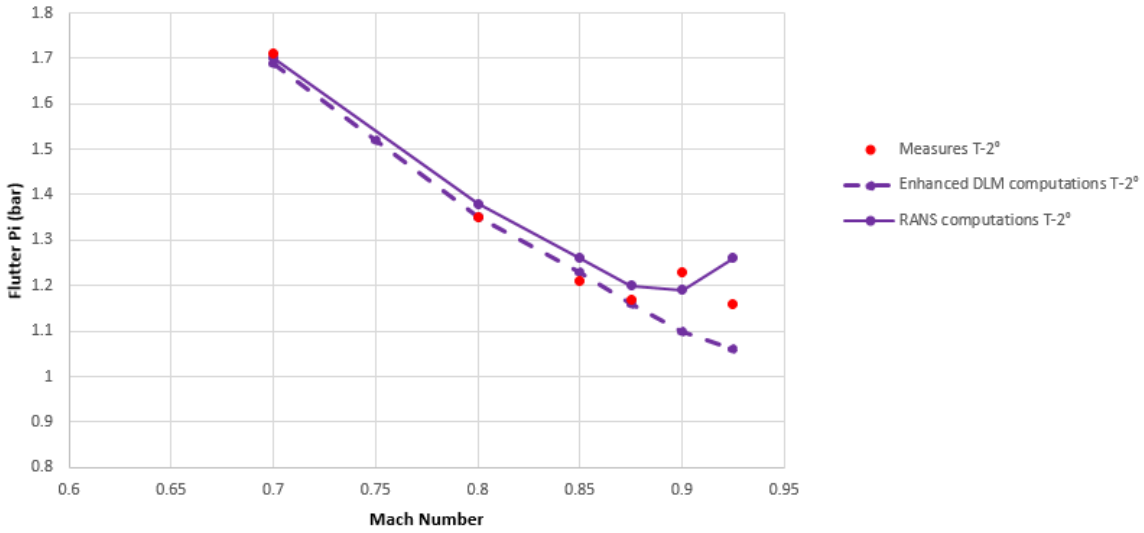

Figure 33 - Flutter restitution for VTP setting -2°(Cz_VTP=0)

4.3.2 T-tail Effects Restitution

The main objective of this test campaign was to gather data to validate numerical predictions of T-tail effects in both subsonic and transonic domains. During the wind tunnel test campaign, the four different tail configurations allowed by the mock-up were tested from Mach 0.7 up to 0.925. The post-processing procedure presented in the previous section was applied to each of the configuration at each Mach number. In total, 38 GVTs, 134 pressure tests and 49 flutter onsets were post-processed to build 17 flutter curves. Figure 34 presents a synthesis of this analysis through the evolution of the flutter critical pressure with Mach number for the different configurations.

The experimental results obtained are in agreement with the van Zyl experiment regarding the decrease of the flutter critical pressure with the increase in the lift of the HTP (defined as VTP on this mock-up for which the flutter critical pressure is higher with the +1° setting than with the -2° or -4° settings). Figure 34 shows a comparison of all experimental data and illustrates the important stabilizing effect of a negative dihedral.

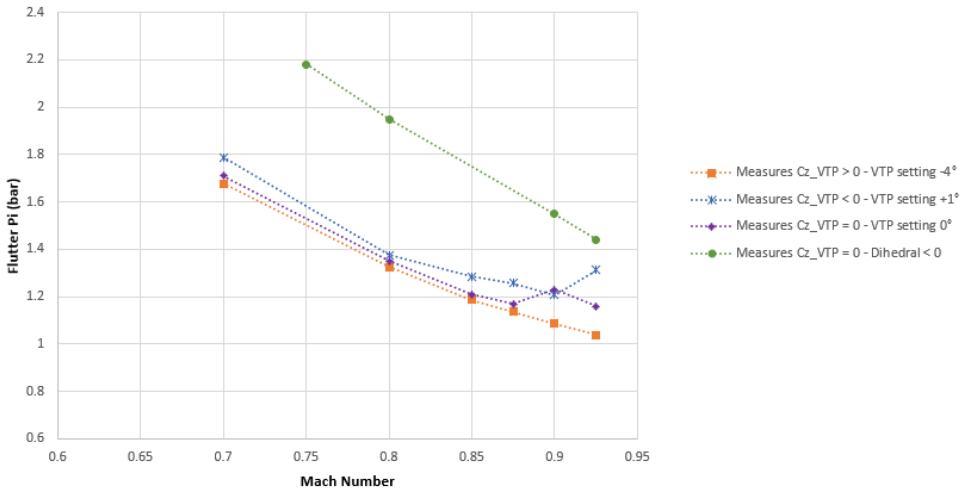

Figure 34 - Experimental results for flutter onsets

Correlations with numerical predictions are good as shown in Figure 35. The enhanced DLM implemented at DASSAULT AVIATION predicts really well the effect of the VTP setting on flutter onset. Numerical and experimental curves are close in subsonic and transonic regions. The dihedral effect prediction is satisfactory even though the correlation between numerical and experimental data is not as good as the correlations for the other curves. For high transonic domain, (Mach 0.9 and above) in the +1° VTP setting, some discrepancy is observed similar to the one observed for the -2° VTP setting in Figure 33. A transonic dip is observed experimentally but this phenomenon cannot be reproduced using the DLM approach. As the DLM is not suited to predict transonic effects, work is currently in progress to use linearized RANS and more precisely an RSM-type turbulence model (DRSM model [10]) to get a correct restitution of this phenomenon.

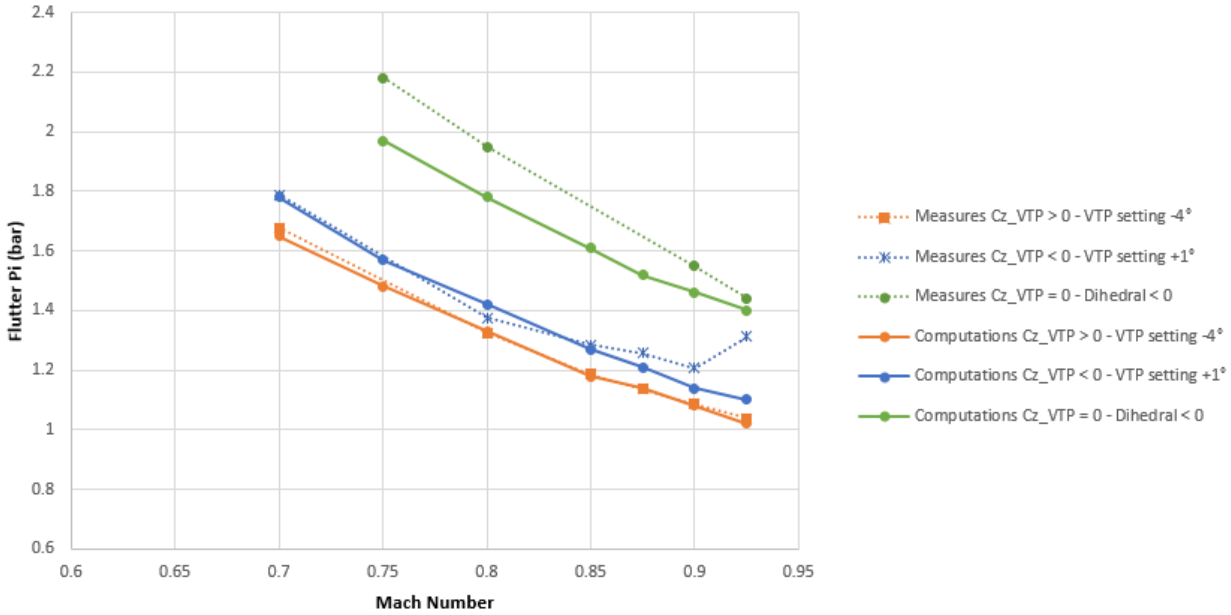

Figure 35 - Flutter prediction correlation with measurements using enhanced DLM

5 CONCLUSIONS

This successful wind tunnel test campaign in 2022 at S2 Modane allowed gathering a large reference database on T-tail flutter in high subsonic and transonic domains. Thanks to GVT data, a good calibration of the finite element model of the flutter mock-up was performed. Steady and unsteady aerodynamic pressure fields were measured for Mach numbers from 0.7 up to 0.925. A good restitution of the pressure tests (harmonic pitching motion of the mock-up) was obtained using DASSAULT AVIATION linearized Navier-Stokes CFD solver *AETHER*. T-tail effects (HTP lift and dihedral effects) and their impact on flutter onset were captured experimentally. These data at high subsonic and transonic Mach numbers enriched the validation of DASSAULT AVIATION in-house enhanced DLM and linearized RANS solvers after their first validation using the van Zyl experiment [5]. Flutter prediction correlations with wind tunnel measurements on a T-tail flutter mock-up were found to be very good. Both enhanced DLM and linearized Navier-Stokes CFD allow an accurate prediction of flutter behavior as they take into account all specific phenomena in T-tail configurations. The experimental database will be used to validate future numerical developments such as the impact of new turbulence models on flutter prediction in the transonic domain.

ACKNOWLEDGEMENTS

The research leading to these results has received funding from the European Union Seventh Framework Programme (FP7/2007-2013) for the Clean Sky Joint Technology Initiative under grant agreement CSJU-GAM-SFWA-2008-001.
This project has received funding from Cleansky-2 Joint Undertaking under the European Union Horizon 2020 research and innovation programme under grant agreement N° CS2-AIR-GAM-2014-2015-01.
This paper only reflects the authors view and the CS2 JU is not responsible for any use that may be made of the information it contains.

The authors would like to thank Louw H. van Zyl for providing the data used for the initial numerical validation of the flutter tools. They also thank Romain Lavanant for his help on the 2022 wind tunnel test restitution during his internship.

REFERENCES

[1] Mamelle H., Broux G., Garrigues E., Wind tunnel flutter tests of a U-tail configuration part 2: experimental and numerical results. *IFASD 2017 Conference Proceeding,* IFASD-2017-124.

[2] Garrigues E., A review of industrial aeroelasticity practices at DASSAULT AVIATION for military aircraft and business jets, *AerospaceLab Journal,* Issue 14 September 2018

[3] Queijo M. J., Theoretical span load distributions and rolling moments for sideslipping wings of arbitrary plan form in incompressible flow, *National advisory committee for aeronautics report 1269,* 1948

[4] Jennings W. P., Berry M. A., Effect of stabilizer dihedral and static lift on T-Tail flutter. *Journal of Aircraft,* 1977

[5] Van Zyl L. H., Mathews E. H., Aerolastic analysis of T-tails using an enhanced Doublet Lattice Method. *Journal of Aircraft,* 2011.

[6] Daumas L., Forestier N., Bissuel A., Broux G., Chalot F., Johan Z., Mallet M., Industrial frequency-domain linearized Navier-Stokes calculations for aeroelastic Problems in the transonic flow regime. *IFASD 2017 Conference Proceeding,* IFASD-2017-050.

[7] Geeraert A., Lepage A., Stephani P., Feldmann D., Häberli W., Wind tunnel flutter tests of a U-tail configuration part 1: model design and testing. *IFASD 2017 Conference Proceeding,* IFASD-2017-072.

[8] Lanari V., Lepage A., Bréus E., T-tail transonic flutter wind tunnel test part 1: Sealing system design and model testing. *IFASD 2024 Conference Proceeding,* IFASD-2024-165.

[9] Bréus E., Huet S., Barber I., Garrigues E., Lubrina P., Stéphan C., Colomies B., Magnier A., Ground vibration test optimization on the Falcon 6X. *IFASD 2022 Conference Proceeding,* IFASD-2022-012.

[10] Martin L., Forestier N., Colo L., Billard F., Chalot F., Johan Z., Mallet M., Extension of linearized CFD methods for complex aerodynamic flows and application to unsteady load evaluations, *IFASD 2022 Conference Proceeding*, IFASD-2022-045.

COPYRIGHT STATEMENT